Supporting Information

Nitrate-nitrite equilibrium in the reaction of NO with Cu-CHA catalyst for NH$_3$-SCR

Christoffer Tyrsted[a], Elisa Borfecchia*[ab], Gloria Berlier[b], Kirill A. Lomachenko[c], Carlo Lamberti[b], Silvia Bordiga[b], Peter N. R. Vennestrøm[a], Ton V. W. Janssens[a], Hanne Falsig[a], Pablo Beato[a], Anna Puig-Molina[a]

[a] Haldor Topsøe A/S, Haldor Topsøes Allé 1, 2800 Kgs. Lyngby, Denmark.
[b] Department of Chemistry, NIS Center and INSTM Reference Center, University of Turin, via P. Giuria 7, 10125 Turin, Italy. * E-mail: elisa.borfecchia@unito.it
[c] IRC "Smart Materials", Southern Federal University, Zorge Street 5, 344090 Rostov-on-Don, Russia

1. NO after NO + O$_2$: evolution of FTIR bands for Cu-nitrates at 100 °C

The experimental results shown in Figure S1 suggest that at 150 °C the desorption rate of adsorbed nitrates (in the experimental conditions of our *in situ* FTIR equipment) is comparable to what observed at 200 °C, and described in the main text. On the contrary, at 100 °C this process is much slower, supporting the hypothesis that nitrites decomposition influences the nitrates/nitrites equilibrium. It is important to stress the fact that the time scale of FTIR experiments cannot be directly compared to either XAS or UV-Vis ones, due to diffusion issues related to physical limitations of the *operando* reactor cell. These include large void volumes, not passing-through flow and catalyst in the form of a thin self-supporting pellet, which make it difficult to homogenize heat and mass within the cell.[1, 2]
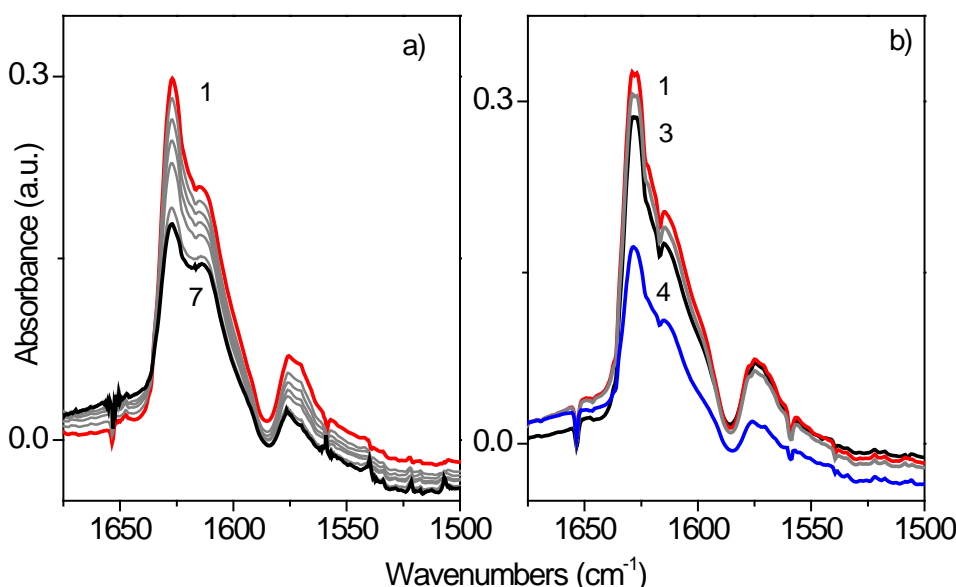
Figure S1. Evolution of Cu(II)-NO$_3^-$ bands during NO/He flow (1000 ppm, 50 ml/min total flow) at a) 150 and b) 100 °C. Spectra 1 (red) were measured immediately after dosing NO. Spectra measured after ca. 150 minutes are number 7 and 3 in panels a) and b) respectively. In the latter, spectrum 4 was measured after 20 h in NO flow.

2. XANES spectra of Cu-CHA prior to reaction of Cu-nitrates with NO
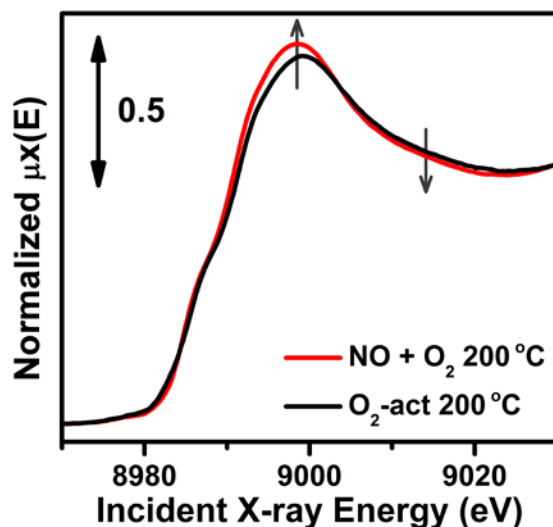
Figure S2. XANES spectra of Cu-CHA sample dehydrated in O_2 at 500 °C and after exposure to NO + O_2 to form the Cu(II)-nitrate. Both spectra were measured at 200 °C.

3. DFT-assisted XANES simulations

XANES simulations performed for Cu-nitrates in both *8r* and *6r* (Figure S3a, top) using exactly the same distances as suggested by DFT resulted in good overall agreement with the experiment, regarding the number and relative intensity of spectral features. However, the calculated spectra appeared to be markedly "squeezed" along the energy axis (Figure S3b). Relative energies of the peaks were significantly improved when a small isotropic contraction was applied to the DFT models. The distance between the features increased in agreement with the Natoli rule,[3] matching those of the experiment (Figure S3c) and confirming the EXAFS fitting results.

Simulated XANES spectra of Cu-nitrate and nitrite species in *8r* are very similar, which demonstrates the value of EXAFS spectroscopy as a tool for the discrimination between them. However, XANES allows to safely disregard a major presence of the N-side configuration for the nitrite species, as simulations give a markedly worse correspondence with experimental data compared to the bidentate O-side configurations.

Figure S3. DFT-assisted XANES simulations of different coordination geometries for Cu-nitrates and Cu-nitrites species inside the Cu-CHA framework. (a) DFT-optimized structures of Cu(II)-NO_3^- and Cu(II)-NO_2^- species considered for the analysis of the Cu-CHA catalyst in the NO+O_2 and NO-only conditions; distances from the Cu centre of the neighboring atoms are also indicated, expressed in Å. (b) Experimental XANES spectra collected for the Cu-CHA at 100 °C in the NO+O_2 and NO-only conditions at 100 °C (thicker curves, top part), compared to simulated XANES spectra for the geometries reported in part (a), using exactly the DFT-optimized bond distances (bottom part, thinner curves). (c) As part (b), but calculating the simulated XANES from bond distances slightly contracted with respect to the DFT minimum (isotropic contraction of 4%).

4. Details on EXAFS fitting

4.1 Model for the EXAFS fit of the Cu-CHA catalyst in the NO + O_2 state (Cu-NO_3^- geometry)

To limit the number of optimized variables, all the SS and MS paths calculated from the Cu-NO_3 *8r* DFT-optimized geometry (see Figure S4a and main text) included in the fitting model have been optimized with the same passive amplitude reduction factor (S_0^2) and with the same energy shift parameter (ΔE). In the fit, the S_0^2 value was set to 0.9, based on the EXAFS analysis of a CuO reference sample.

The parameterization of the EXAFS paths was performed distinguishing the Cu coordination to the zeolite framework and to the NO_3^- or NO_2^- groups. In particular, for the Cu coordination to the zeolite framework, the SS paths involving the first-shell **O_{fw}** atoms and the second-shell **Al_{fw}** atom were included with specific radial shift (ΔR) and Debye Waller (DW, σ^2) parameters. A lower-level parametrization strategy has been then adopted for the SS paths which involve the **Si/O fw** atoms falling in the (2.8 – 3.5) Å distance range from the Cu center. These SS paths were modeled considering a common contraction/expansion factor α_{fw} and a DW factor σ^2_{fw} increasing as the square root of the distance $R_{eff,i}$ of the ith scattering atom from the absorber ($\Delta R_{fw,i} = \alpha_{fw} R_{eff,i}$, $\sigma^2_{fw,i} = \sigma^2_{fw} (R_{eff,i})^{1/2}$; optimized parameters: α_{fw}, σ^2_{fw}).

The NO_3^- and NO_2^- groups have been considered as rigid units (internal bond distances fixed to DFT-values), with a translational degree of freedom along the **Cu–N** axis. As schemed in Figure S4a, the first shell bond distance **Cu–O1** has been directly optimized in the fit, whereas the second-shell distance **Cu–N** and, for nitrates only, the third-shell **Cu–$O2_{NO3}$** distance have been derived from geometrical considerations (resulting in the following relations: $\Delta R_N = \approx 1.179 \cdot \Delta R_{O1}$; $\Delta R_{O2(NO3)} = \Delta R_N$)

The EXAFS signal in the (2.5 – 3.5) Å R-space region is dominated by MS contributions. In particular, coordination of both nitrates and nitrites groups in the chelating bidentate configuration results in moderately strong MS contributions along the **O_{fw}–Cu–O1** bond axis (indicated by the white arrow in Figure S4b). A second set of *very* strong MS contributions is instead a fingerprint for bidentate nitrates structures, involving the second-shell nitrogen **N** and the most distant O atom **$O2_{NO3}$** of the NO_3^- group, along the **Cu–N–$O2_{NO3}$** bond axis (green arrow in Figure S4b).

Each SS path was parameterized with its own DW factor, except for SS paths including the **N** and **$O2_{NO3}$** atoms of the nitrate group, optimized with the same DW. In addition, an independent DW was optimized for all the MS paths included in the fit model.
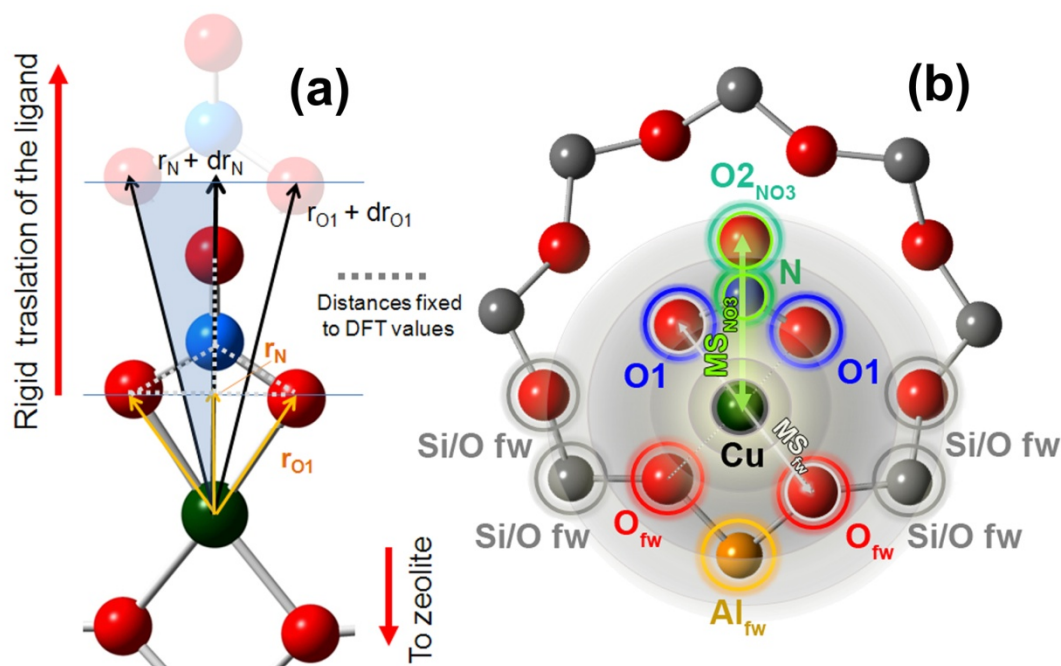
Figure S4. Identification of chelating bidentate Cu-nitrates by EXAFS fitting. (a) Geometrical assumptions adopted to perform the fits of the EXAFS spectra relevant to the nitrate/nitrite equilibrium on the Cu-CHA catalyst. (b) Scheme of the principal single scattering (SS) and multiple scattering (MS) paths contributing to EXAFS signal in the (1.0 – 3.8) Å R-space range, included in the fitting model. The DFT-optimized structure of the Cu(II)-NO$_3^-$ complex in the chelating bidentate configuration hosted in the 8r unit of the *cha* framework (see Figure 3a in the main text) has been adopted as initial guess in the EXAFS fit procedure.

4.2 Details on two-component EXAFS fit of the NO-only state

The two-component fit of the NO-only state was performed setting the scattering amplitude for the two sets of paths calculated from DFT-optimized geometries to the S_0^2 value of 0.9 derived from the analysis of a CuO standard (as in the previous fit for the NO + O$_2$ spectrum with the Cu-NO$_3^-$ geometry only), weighted for the percentage of each component (#$_{NO3}$: percentage for the Cu-NO$_3^-$ geometry; $(1 - $#$_{NO3}) = $#$_{NO2}$: percentage for the Cu-NO$_2^-$ geometry), with #$_{NO3}$ being optimized in the fit. A common set of parameters was employed for both the Cu(II)-NO$_3$ and the Cu(II)-NO$_2$ component (radial shift parameters and DW factors), on the basis of their strong structural similarity up to the second Cu-coordination shell. The Cu(II)-NO$_3$ component is however discriminated by the additional scattering paths involving the O2$_{NO3}$ atom, including the scarcely contributing O2$_{NO3}$ SS path and the high-intensity collinear MS paths, MS$_{NO3}$, the latter parametrized with a specific DW factor $\sigma^2_{MS(NO3)}$. Optimized values of the fit parameters are reported in Table 1 (main text). The 2-component fit yielded a very good reproduction of the experimental spectrum, with physically reliable values of all the refined parameters. In general, for the paths involving the NO$_3^-$/NO$_2^-$ units, DW factors slightly higher with respect to the Cu-nitrate only case (NO + O$_2$ experimental spectrum) are observed, as expected in correspondence of two different Cu-species coexisting in the catalyst.

4.3 Experimental and best fit XAS spectra in k-space

The experimental k^{2}χ(k) EXAFS spectra obtained at 100 °C under NO + O$_2$ (red) and NO feed (blue) are compared in Figure S5a. Consistently with the structural interpretation presented in the main text, we can appreciate small but significant differences in the amplitude and frequency of the

EXAFS oscillations collected for the NO + O_2 and NO conditions (in the whole analyzable k-range, from 2.5 to 12.4 $Å^{-1}$. These are well reproduced by the best fit curves (orange and light blue lines for NO + O_2 and NO feed, respectively) obtained as described in the previous Section and in the main text.

The differences in the $k^2\chi(k)$ curves can be further evidenced by calculating differential spectra $\Delta k^2\chi(k) = [k^2\chi(k)_{NO+O2}] - [k^2\chi(k)_{NO}]$ from the experimental and best fit spectra (black and gray line in Figure S5b, respectively). The experimental $\Delta k^2\chi(k)$ results in a well-structured oscillatory signal, in good agreement with the best fit differential curve accounting for the conversion of Cu-nitrates to Cu-nitrates in ca. 60% of the Cu-sites. This allowed us to safely exclude that the differences in the FT EXAFS spectra could be due to high-k noise or other artifacts connected to the Fourier transform operation.
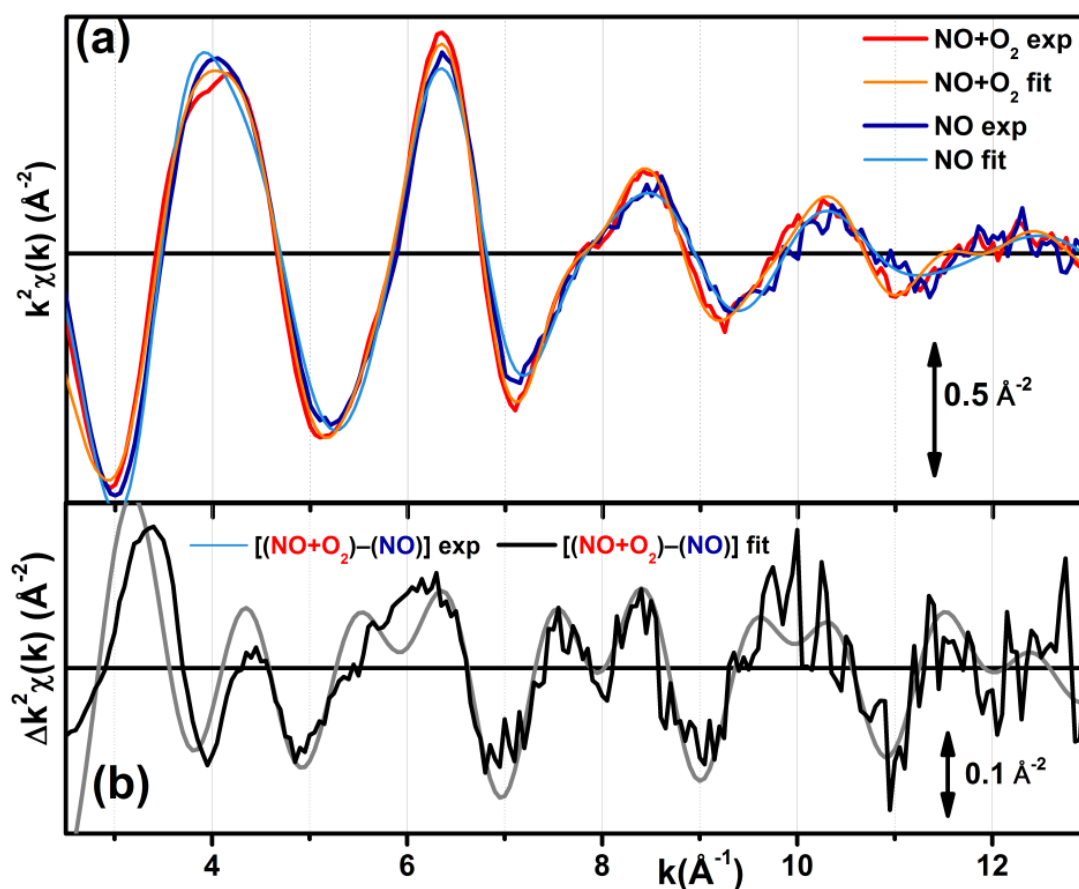
Figure S5: (a) Experimental $k^2\chi(k)$ EXAFS spectra obtained at 100 °C under NO + O_2 feed (red) and NO feed (blue) and correspondent best fit curves (orange and light blue lines, for NO + O_2 and NO feed, respectively). (b) Experimental differential $k^2\chi(k)$ EXAFS spectra calculated as: $\Delta k^2\chi(k) = [k^2\chi(k)]_{NO+O2} - [k^2\chi(k)]_{NO}$ (black) compared to the best fit one (gray), obtained from the difference between orange and light blue curve in part (a).

The principal difference observed between FT EXAFS spectra for the NO + O_2 and NO condition (see Figure 3d in main text) is observed in the (2.8–3.6) Å range, in correspondence of the third maximum in the |FT| spectra at ca. 3 Å. To further investigate origin of such difference in R-space, we back Fourier transformed the k^2-weighted FT spectrum of the Cu-CHA catalyst exposed to NO + O_2 feed in the (2.8–3.6) Å range (see Figure S6 inset). The back-Fourier-transformed experimental spectrum, $Re[\chi(q)]_{exp}$, and the correspondent best fit curve, $Re[\chi(q)]_{fit}$, are reported in

Figure S6 (orange thick and purple thin lines, respectively). The amplitude of the oscillations for back-FT spectrum is still a significant contribution to the global $k^2\chi(k)$ EXAFS spectrum (red curve in Figure S6), well above the noise level. It is optimally reproduced by the best fit line accounting for chelating bidentate Cu-nitrates as dominant component in the NO + O_2 catalyst state. Moreover, the EXAFS signal coming from the (2.8–3.6 Å range is clearly a major contribution to the best fit differential $\Delta k^2\chi(k)_{fit}$ curve (gray dashed line in Figure S6) modeling the differences between the NO + O_2 and the NO catalyst states. In particular, the frequency modulation of $\Delta k^2\chi(k)_{fit}$ curve from 3.5 Å^{-1} is perfectly reproduced by the $Re[\chi(q)]$ curve. Hence, k-space analysis supports that the partial lack of NO_3 MS paths falling in the (2.8–3.6 Å range plays a key role in determining the experimentally detected differences, whereas in the shorter R-space range the structural contrast between the two configurations is lower.
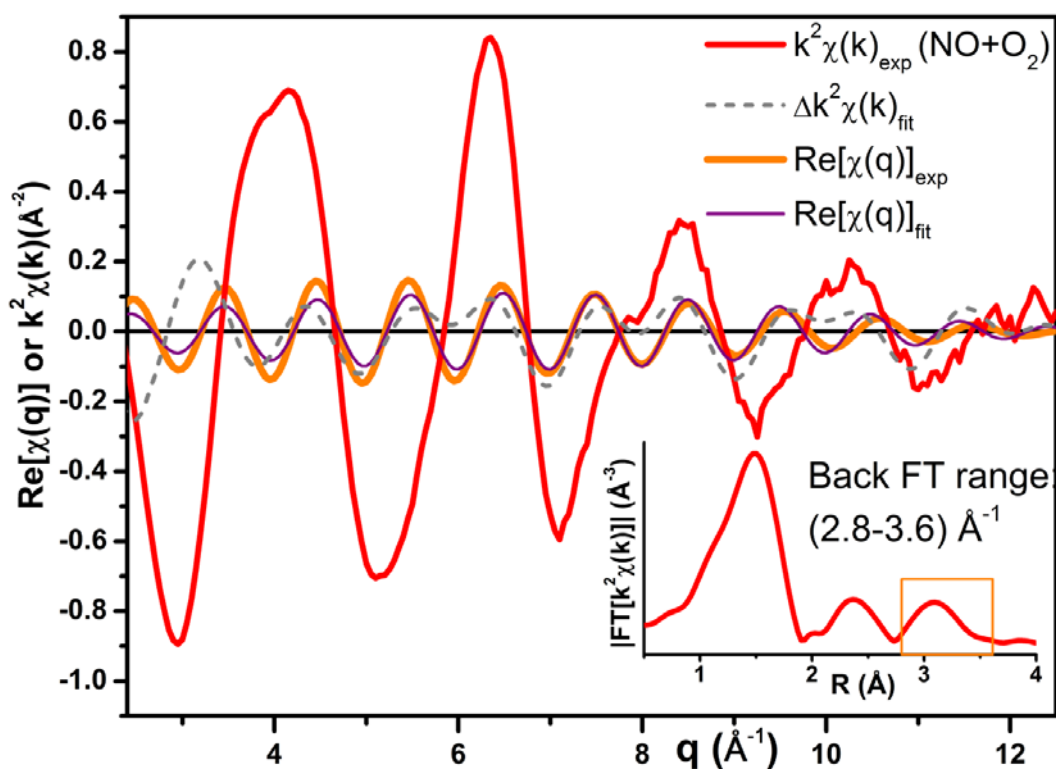
Figure S6: Back Fourier Transform in the (2.8–3.6) Å range of the experimental k^2-weighted FT spectra of the Cu-CHA catalyst exposed to NO + O_2 feed range, highlighted by the orange box in the inset ($Re[\chi(q)]_{exp}$, orange line) and the correspondent best fit curve ($Re[\chi(q)]_{fit}$, purple line). The experimental $k^2\chi(k)$ EXAFS (red line) and the differential best fit spectrum calculated as $\Delta k^2\chi(k) = [k^2\chi(k)]_{NO+O2} - [k^2\chi(k)]_{NO}$ (gray dashed line) are also reported for comparison.

5. EXAFS tests on hypothetical monodentate Cu(II)-NO$_2$ species

As discussed in main text, the possibility of having a monodentate Cu(II)-NO$_2$ with Cu coordinating to the N-side of the nitrite (Figure S3a, Cu-NO$_2$-Nside *8r* and *6r* structures) was also considered as an alternative to formation of chelating bidentate Cu-nitrites.

The theoretical XANES obtained from these structures, hosted in both *6r* and *8r* rings of the CHA framework, leads to different features compared to the bidentate nitrite species which does not appear to be present in the measured XANES (Figure S3b,c, green curves).

Furthermore, using the Cu-NO$_2$-Nside *8r* and *6r* structures for EXAFS analysis does not yield satisfactory results as illustrated in Figure S7. The figure reports for each geometry a "simulation" of the EXAFS signal obtained by "freezing" all bond distances to the DFT values (*i.e.* setting all ΔR_i parameters to zero), and by setting all the other fit parameters (S_0^2, ΔE, DWs) to the values reported in the main text (Table 1) refined in the successful fit of the NO + O$_2$ state with the Cu-NO$_3$ *8r* geometry.

For both geometries, a lack in coordination number and a strong antiphase between the SS paths involving the nearest Cu neighbors (1 **N$_{NO2}$** at ca. 1.9 Å, 2 **O$_{fw}$** at 2.0−2.1 Å, 1 **O2$_{NO2}$** for *8r* or 1 **O$_{fw}$** for *6r* at ca. 2.3−2.4 Å) is observed, which results in a critical damping of the first shell signal in evident disagreement with the experimental datum. Also in the second shell region, both structures are unable to satisfactorily reproduce the experimental EXAFS signal.

The third maximum cannot be reproduced at all, confirming that this EXAFS feature is a unique fingerprint of Cu-nitrates in the chelating bidentate coordination mode, partially unreacted in the NO-only state.
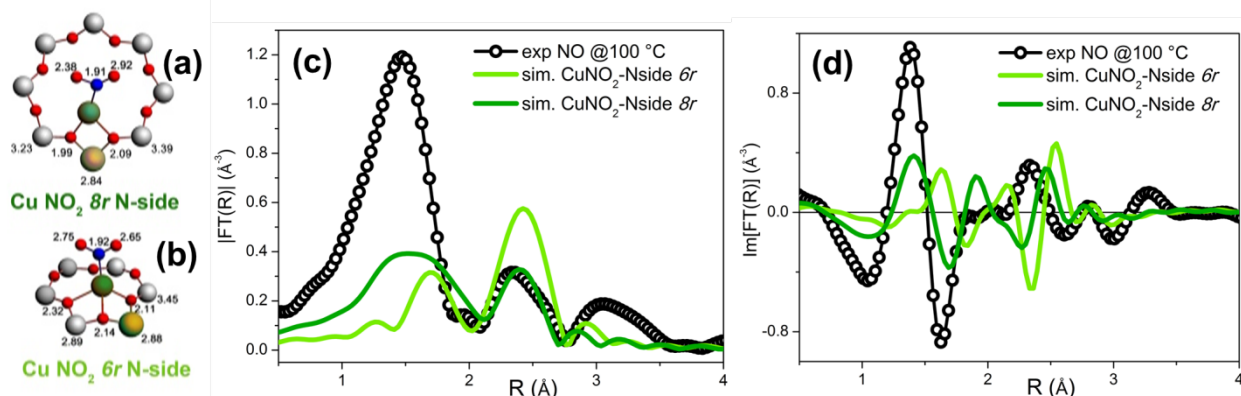
Figure S7. Magnitude (c) and imaginary part (d) of the experimental FT EXAFS spectra (black circles) obtained under NO feed and corresponding EXAFS simulations (solid lines), based on the monodentate Cu(II)-NO$_2$ species in the *6r* (structure in part (a), light green lines) and *8r* (structure in part (b), dark green curves).

Albeit differences in the optimal parameters values are plausible in connection with differences in the bidentate and monodentate coordination modes (especially DW values for the scattering paths involving nitrite group), these are expected to be of limited entity, and their impact on simulated signal is undoubtedly insufficient to achieve a satisfactory level of reproduction of the experimental features.

Remarkably, conventional fits performed on the basis of these geometries, guessing the whole set of parameters, drastically failed, resulting in several negative DWs and unreliable radial shift values (< 0.15 Å) from the DFT minima.

These results allow us to safely rule out the presence of a significant fraction of monodentate nitrites as the second component present together with unreacted bidentate nitrates in the experimentally probed NO-only state.

References

1.   M. A. Banares, *Catal. Today*, 2005, **100**, 71-77.
2.   B. M. Weckhuysen, *Physical Chemistry Chemical Physics*, 2003, **5**, VI-VI.
3.   C. R. Natoli, in *EXAFS and Near Edge Structure*, eds. A. Bianconi, L. Incoccia and S. Stipcich, Springer Verlag, 1983, p. 43.